# Ab Initio Study of Selective Fluorescence Quenching of Polycyclic Aromatic Hydrocarbons

**John V. Goodpaster,† James F. Harrison, and Victoria L. McGuffin***

*Department of Chemistry and Center for Fundamental Materials Research, Michigan State University, East Lansing, Michigan 48824-1322*

*Received: June 19, 2002*

The mechanism of selective fluorescence quenching of alternant polycyclic aromatic hydrocarbons (PAHs) by nitromethane has been investigated using ab initio calculations. Initial studies using 10 archetypal configurations of pyrene (an alternant PAH) and nitromethane established trends in the attractive and repulsive interactions between the two molecules. In general, the computed energy of interaction in the ground and excited states correlated with the orientation of the dipole moment of nitromethane with respect to the electrostatic potential of pyrene. In addition, many local minima were found on the potential energy surface; hence, two representative configurations (one attractive and one repulsive) were explored in detail. Calculations of the interaction of pyrene and fluoranthene (a nonalternant isomer of pyrene) with nitromethane were also conducted as a function of intermolecular separation distance. Two main routes were found for deactivation of the excited-state PAHs by nitromethane: direct energy transfer to the quencher or formation of a fluorophore−quencher ion pair. In studies of their various excited states, pyrene showed an energetically feasible path to an ion pair, whereas fluoranthene did not. In addition, simulation of PAH−solvent complexes showed that neither isomer formed energetically reasonable ion pairs with acetonitrile. Therefore, the selectivity of nitromethane for pyrene appears to be based on the relative ease with which these molecules form an ion pair and then undergo back electron transfer to regenerate the ground state.

## I. Introduction

Polycyclic aromatic hydrocarbons (PAHs) are a large and diverse family of organic compounds composed solely of carbon and hydrogen. PAHs consist of two or more fused aromatic rings in many and varied configurations, where the number of stable isomers increases dramatically with the number of aromatic rings. These compounds are both naturally occurring and anthropogenic, having environmental, toxicological, and astronomical importance.[1−3]

PAH isomers can be organized into two main classes. To distinguish between them, each carbon atom in the aromatic structure is labeled, alternately skipping an atom between labels. Alternant PAHs (e.g., pyrene) have a structure such that no two atoms of the same type (labeled or unlabeled) are adjacent. Nonalternant PAHs (e.g., fluoranthene) have a structure in which such labeling results in two adjacent atoms of the same type. These structural differences can result in large changes in the physical, chemical, spectroscopic, and toxicological properties. Given the importance and structural diversity of PAHs, it is highly desirable to be able to differentiate between alternant and nonalternant isomers. Among the analytical techniques used for the determination of PAHs, luminescence spectroscopy offers high sensitivity and selectivity and is widely applicable to many samples.[4−14] However, luminescence techniques are not always sufficiently selective for the analysis of PAH isomers in complex samples.

Fluorescence quenching is one approach that may provide the requisite sensitivity and selectivity for PAH analysis. Previous experimental work has shown that nitromethane selectively quenches the fluorescence from alternant PAHs over nonalternant PAHs.[15] Subsequent quantitative measurements have shown that alternant isomers are quenched 100−1000 times more effectively than nonalternant isomers.[16−18] However, the continued development of selective quenching for PAH analysis has been relatively limited. This lack of progress is mainly due to incomplete understanding of the mechanism for fluorescence quenching and the consequent inability to identify promising quenching agents without time-consuming, trial-and-error experimentation. The most widely accepted theory for selective quenching of alternant and nonalternant PAHs presumes an electron-transfer mechanism, where the fluorophore serves as an electron donor or acceptor in a charge-transfer complex with the quencher.[19] In this mechanism, the fluorophore and quencher form an encounter complex in solution, followed by partial or full electron transfer. This is followed by a rapid back electron transfer, which returns both quencher and fluorophore to their ground states. Using the Hückel approximation, the highest occupied molecular orbital (HOMO) and lowest unoccupied molecular orbital (LUMO) of alternant PAHs have higher one-electron energies than their nonalternant isomers.[20] Because the LUMO of an electron-accepting quencher such as nitromethane is assumed to lie at a lower energy than the LUMO of the alternant PAH that is serving as the electron donor,[21] Hückel theory predicts that an excited-state alternant PAH should undergo electron transfer with nitromethane more readily than an excited-state nonalternant isomer.

Although this model for the selectivity of fluorescence quenching seems intuitively reasonable, it has not been confirmed experimentally. For example, ionization energies and reduction potentials of PAHs (which would presumably reflect electron donating or accepting ability) have not been good empirical predictors of quenching efficiency.[16,17] In addition, this model considers only the electronic properties of the

* To whom correspondence should be addressed. Phone: 517-355-9715 ext. 244. Fax: 517-353-1793. E-mail: jgshabus@aol.com.

† Current address: Bureau of Alcohol, Tobacco, and Firearms, Department of the Treasury, Rockville, MD 20850.

10.1021/jp021454g CCC: $22.00 
Published on Web 10/05/2002

fluorophore and not the quencher to be important to the quenching mechanism. This model cannot quantitatively predict quenching efficiencies, nor does it account for the numerous PAHs that possess an alternant or nonalternant structure but do not exhibit the expected quenching behavior. Previous ab initio calculations (HF/6-31G*) have shown that pyrene and fluoranthene adhere to the HOMO/LUMO trend discussed above, whereas benzo(*a*)pyrene and benzo(*b*)fluoranthene do not.[22] Moreover, the LUMO energy of nitromethane at this level of theory is higher than the LUMO energy of any of the above PAHs (in the gas phase). All of these discrepancies suggest that the current model is not an adequate or sufficient description of the selective quenching process.

The use of ab initio quantum mechanics to study this phenomenon is attractive as such methods may provide an in-depth view and increased understanding of the photophysical processes that underlie fluorescence quenching. To date, ab initio calculations have been used to predict geometries,[23−26] heats of formation,[27−30] vibrational frequencies,[31−33] charge distributions, and ionization energies[34] of ground-state PAHs. For excited states, the Pariser−Parr−Pople (PPP) approximation has been applied to the calculation of PAH electronic spectra.[35−37] Other semiempirical methods have also been used for excited-state PAHs[38−41] as well as their ions and derivatives.[42−45] More recently, time-dependent density functional theory has been applied to the calculation of PAH excitation energies.[46] Finally, other excited-state properties such as charge distributions[47] and vibrational frequencies[48] have been calculated.

Previous calculations by Goodpaster et al. have established clear differences in the ground- and excited-state properties of alternant and nonalternant PAHs.[22] In this work, good agreement was observed between the computed ground-state geometries and experimental data from neutron diffraction. In addition, ground- and excited-state vibrations were accurately predicted. Interestingly, the ground-state geometries of nonalternant isomers contained five-membered rings whose bonds were not fully conjugated with the aromatic $\pi$ system. Upon reaching an excited state, these aliphatic C−C bonds tended to contract more than the aromatic C−C bonds in other parts of the molecule, which accounts for the lack of vibrational fine structure in the emission spectra of these molecules.[22,49] Furthermore, the excited states of nonalternant PAHs were generally at lower energy relative to the ground state when compared to their alternant isomers.

In recent years, there has been significant interest in studying both ground- and excited-state charge-transfer reactions using computational techniques.[50−53] Nevertheless, published calculations involving complexes between PAHs and other chemical species have not been as well developed as those for individual PAH molecules. Semiempirical methods have been used to study the ground- and excited-state structures of some PAH charge-transfer complexes.[54−56] The majority of work in this area has not involved large PAH molecules nor the transient excited-state complexes that are characteristic of selective quenching reactions. The development of a theoretical model for selective fluorescence quenching would allow the computational evaluation of novel quenchers and help to direct experimental efforts. Toward that end, this study has examined energy and electron transfer in various fluorophore−quencher and fluorophore−solvent complexes involving the PAHs pyrene and fluoranthene, the quencher nitromethane, and the solvent acetonitrile.

## II. Methods

Ground- and excited-state calculations use the Gaussian 98[57] program on a SGI Origin 2400 with thirty two 300 MHz R12000 processors and a CRAY T90. All ground-state calculations use the Hartree−Fock (HF) method, whereas excited states are treated using configuration interaction with single excitations (CIS). The geometries of all molecules are optimized individually at the HF/6-31G* level while constrained to the following point groups: pyrene ($D_{2h}$), fluoranthene ($C_{2v}$), nitromethane ($C_s$), and acetonitrile ($C_{3v}$).

Partial optimizations are performed wherein the molecular geometries are held constant while the relative separation distance and orientation of the molecules are varied. An initial study of the pyrene−nitromethane system uses 10 archetypal configurations where a plane of symmetry is preserved for an overall $C_s$ point group. Subsequent studies use two configurations (one attractive and one repulsive) for each molecular complex with a custom basis set. In these calculations, a 6-31G basis set is used for the atoms of the fluorophore molecule, whereas a 6-31+G basis set is used for the atoms of the quencher or solvent molecule in order to simulate more adequately the diffuse electron density characteristic of an anion. In all calculations, the energies and properties of the ground state and 10 lowest singlet and triplet excited states are determined as a function of intermolecular separation distance.

## III. Results and Discussion

**A. Effect of Molecular Orientation.** A total of 10 representative configurations of pyrene and nitromethane are shown in Figure 1. To provide an initial and qualitative comparison of these various configurations, the interaction energy is calculated at the HF/3-21G level and basis set superposition error is neglected. In these calculations, the molecules are held in their optimum ground-state geometries while the intermolecular separation distance is varied. The interaction energy is defined as the difference between the energy of the pyrene−nitromethane complex at its optimum separation distance and the energy of the isolated molecules. These calculations, summarized in Table 1, demonstrate that the interaction energy is dominated by the relative orientation of the dipole moment of nitromethane with respect to the electrostatic potential of pyrene. Nitromethane is a highly polar molecule, with a calculated dipole moment (4.2 D at the HF/3-21G level) that is directed along the C−N bond axis toward the negative nitro group. The configurations where this dipole moment is oriented toward the positive electrostatic potential of the hydrogen atoms on pyrene (i.e., A, B, and C) are the most stable. The configurations where this dipole moment is oriented in the opposite direction (i.e., H, I, and J) are the least stable. In configurations such as these, the optimized intermolecular separation distance is very large, and the energy of the molecular complex is slightly higher than that of the separated molecules. We believe these local minima reflect the competition between the long-range, repulsive dipole interaction and the shorter-range, attractive induced-dipole/dipole interaction, both of which succumb to the larger Pauli repulsion as the separation distance between the molecules decreases. It is also noteworthy that the interaction energies for the ground-state complexes are similar to those for the excited-state complexes, which indicates that the dipole moment of nitromethane and the electrostatic potential of pyrene do not change substantially upon excitation.

For the ground-state complexes, optimization of all intermolecular variables results in various final configurations, all of which are similar to A, B, C, or D in Figure 1. The precise final location of the optimized molecules depends on their initial location. This suggests that, although there is a substantial driving force for the association of the nitro group of nitro-

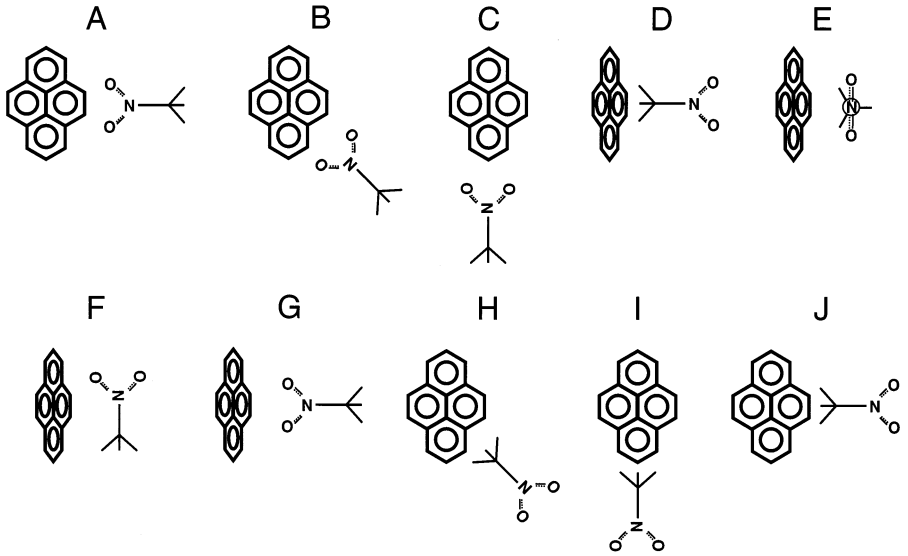


**Figure 1.** Representative configurations of the pyrene−nitromethane complex. All complexes are constrained to $C_s$ symmetry.

**TABLE 1: Interaction Energy ($E_a$)[a] for the Ground-State Pyrene−Nitromethane Complex ($^1P_0 + {}^1N_0$)**

| configuration[b] | $E_a$ (eV) | configuration[b] | $E_a$ (eV) |
|---|---|---|---|
| A | −0.2669 | F | −0.0816 |
| B | −0.2623 | G | 0.0006 |
| C | −0.2475 | H | 0.0007 |
| D | −0.1412 | I | 0.0126 |
| E | −0.0977 | J | 0.0158 |

[a] Interaction energy is difference between energy at optimum intermolecular separation distance and energy of isolated molecules (HF/3-21G). [b] See Figure 1.

methane with the hydrogen atoms of pyrene, there are multiple local minima on the potential energy surface of the pyrene−nitromethane system. Accordingly, two representative configurations, one attractive (A) and one repulsive (G), are used in further studies. This approach is appropriate given that excited-state quenching interactions are thought to be transient and collisional in nature, allowing many possible orientations of the two molecules as they randomly diffuse together in solution.

**B. Effect of Basis Set and Basis Set Superposition Error.** The effect of basis set on the relative energies of the singlet excited states of the pyrene−nitromethane ($^1P_x + {}^1N_y$) and fluoranthene−nitromethane ($^1F_x + {}^1N_y$) complexes is shown in Figures 2 and 3, respectively. Both complexes are held in configuration A with an intermolecular separation distance of 2.0 Å. In order of increasing energy relative to the ground state ($^1P_0 + {}^1N_0$), Figure 2 shows the first two singlet excited states of pyrene ($^1P_1 + {}^1N_0$ and $^1P_2 + {}^1N_0$), the first two singlet excited states of nitromethane ($^1P_0 + {}^1N_1$ and $^1P_0 + {}^1N_2$), and the third singlet excited state of pyrene ($^1P_3 + {}^1N_0$). In addition, a singlet ion-pair state ($^2P^+ + {}^2N^-$) is seen, which is of particular interest as transitions to this state from other excited states have been implicated in the mechanism for fluorescence quenching.[19,21] The analogous states for the fluoranthene−nitromethane complex are shown in Figure 3.

Overall, and as expected, there is a large decrease in the excitation energies of both complexes as the basis set is expanded. More importantly, however, the energies of the various excited states change relative to one another. In particular, the energy of the lowest-lying ion-pair state of pyrene−nitromethane decreases dramatically with respect to the adjacent singlet excited state of pyrene ($^1P_3 + {}^1N_0$). In fact, this decrease is sufficient at the CIS/6-31G level to make the

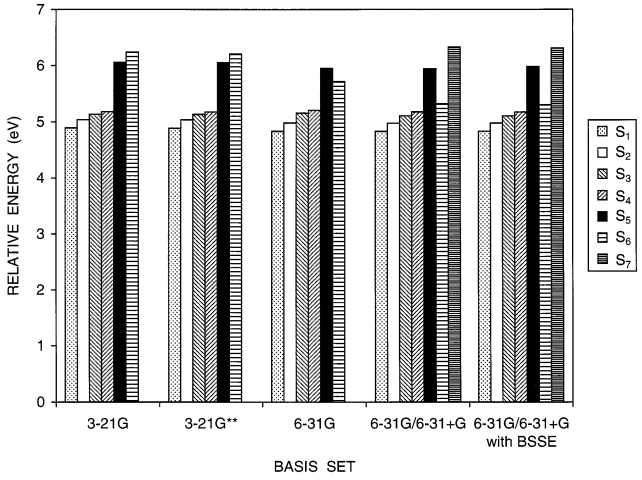


**Figure 2.** Effect of basis set on the relative energies of the excited states of the pyrene−nitromethane complex (configuration A, 2.0 Å intermolecular separation distance). States: (see legend to right of figure) $S_1 = {}^1P_1 + {}^1N_0$, $^1A'$ symmetry; $S_2 = {}^1P_2 + {}^1N_0$, $^1A'$ symmetry; $S_3 = {}^1P_0 + {}^1N_1$, $^1A''$ symmetry; $S_4 = {}^1P_0 + {}^1N_2$, $^1A''$ symmetry; $S_5 = {}^1P_3 + {}^1N_0$, $^1A'$ symmetry; $S_6 = {}^2P^+ + {}^2N^-$, $^1A'$ symmetry; $S_7 = {}^2P^+ + {}^2N^-$, $^1A'$ symmetry.

ion pair less energetic than $^1P_3 + {}^1N_0$ at the separation distance studied. Notably, this behavior is not seen with fluoranthene−nitromethane. Adding diffuse (+) functions to the atoms of nitromethane further lowers the energy of this ion pair and results in the appearance of a new ion-pair state for both the pyrene−nitromethane and fluoranthene−nitromethane systems. Therefore, a mixed 6-31G/6-31+G basis set is applied in the remaining studies in order to represent the anionic character of the quencher in the ion pair more accurately.

Because these systems are molecular complexes, the effect of basis set superposition error (BSSE) must also be considered. BSSE arises because the basis set of the complex is more spatially extensive than that of the isolated molecules, such that their energies cannot be directly compared. The traditional approach for calculating and removing BSSE is to use an a posteriori method known as the Boys−Bernardi or counterpoise method.[58−60] In this method, separate calculations are performed for the isolated molecules using the basis set for the entire complex. These energies are then subtracted from the energy of the complex to determine the BSSE-corrected interaction

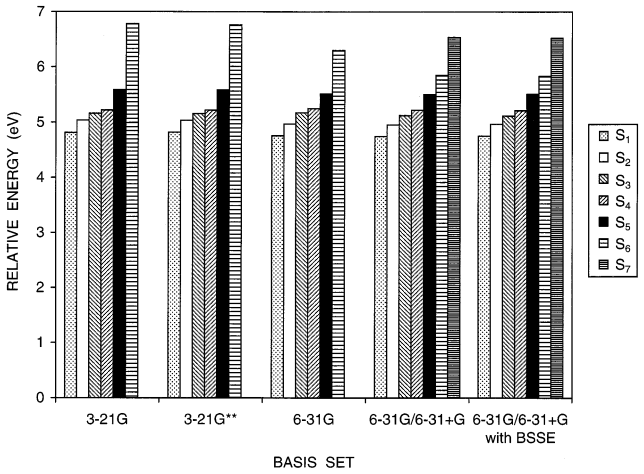


**Figure 3.** Effect of basis set on the relative energies of the excited states of the fluoranthene−nitromethane complex (configuration A, 2.0 Å intermolecular separation distance). States: (see legend to right of figure) $S_1 = {}^1F_1 + {}^1N_0$, $^1A'$ symmetry; $S_2 = {}^1F_2 + {}^1N_0$, $^1A'$ symmetry; $S_3 = {}^1F_0 + {}^1N_1$, $^1A''$ symmetry; $S_4 = {}^1F_0 + {}^1N_2$, $^1A''$ symmetry; $S_5 = {}^1F_3 + {}^1N_0$, $^1A'$ symmetry; $S_6 = {}^2F^+ + {}^2N^-$, $^1A'$ symmetry; $S_7 = {}^2F^+ + {}^2N^-$, $^1A'$ symmetry.

energy. This process is repeated at each intermolecular separation distance in order to generate the BSSE-corrected potential energy surface. These a posteriori corrections should be seen as a crude estimate of the error and not an upper bound.

In the case of pyrene−nitromethane and fluoranthene−nitromethane, the magnitude of the BSSE correction varies with the state of interest. For example, the BSSE correction for the ground and first seven singlet excited states of pyrene−nitromethane ranges from −0.04 to −0.09 eV at a separation distance of 2.0 Å. Similarly, the BSSE correction for fluoranthene−nitromethane ranges from −0.05 to −0.08 eV. In general, the correction was relatively similar for all of the neutral excited states and smallest for the ion pairs. However, these corrections represent a very small fraction of the excitation energy, ranging from +0.57 to −0.33% for pyrene−nitromethane (Figure 2) and +0.24 to −0.27% for fluoranthene−nitromethane (Figure 3). There is no change in the order of the excited states and little change in their relative energies. As a consequence, BSSE corrections have not been included in subsequent calculations.

**C. Singlet-State Potential Energy Surfaces.** *1. PAH−Nitromethane Complexes.* As previously mentioned, two configurations (A and G, Figure 1) have been chosen to generate singlet-state potential energy surfaces using a 6-31G/6-31+G basis set. The energies of the PAHs with either nitromethane or acetonitrile are calculated as a function of intermolecular separation distance and are shown in Figures 4−11. It is important to note that all of these pseudo one-dimensional potential curves are the adiabatic curves obtained directly from the CIS calculations and, although these curves cannot describe the various crossings as accurately as the corresponding diabatic curves, they do provide considerable qualitative insight.

Figures 4 and 5 show the interaction of pyrene and nitromethane in configurations A and G, respectively. In both cases, a number of curves that represent the energies of various excited states are displayed. At large separation distances, the states represented in order of increasing energy are as follows: excited-state pyrene with ground-state nitromethane (${}^1P_1 + {}^1N_0$, ${}^1P_2 + {}^1N_0$, ${}^1P_3 + {}^1N_0$, and ${}^1P_4 + {}^1N_0$), ground-state pyrene with excited-state nitromethane (${}^1P_0 + {}^1N_1$ and ${}^1P_0 + {}^1N_2$), and two ion pairs consisting of a pyrene cation with a nitromethane anion (${}^2P^+ + {}^2N^-$).

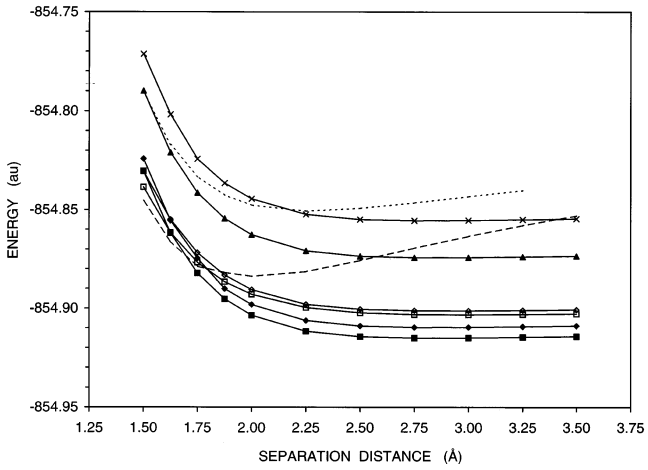


**Figure 4.** Interaction of pyrene (P) with nitromethane (N) in configuration A. States: (■) $S_1 = {}^1P_1 + {}^1N_0$, $^1A'$ symmetry; (◆) $S_2 = {}^1P_2 + {}^1N_0$, $^1A'$ symmetry; (□) $S_3 = {}^1P_0 + {}^1N_1$, $^1A''$ symmetry; (◇) $S_4 = {}^1P_0 + {}^1N_2$, $^1A''$ symmetry; (▲) $S_5 = {}^1P_3 + {}^1N_0$, $^1A'$ symmetry; (X) $S_6 = {}^1P_4 + {}^1N_0$, $^1A'$ symmetry; (− − −) $S_7 = {}^2P^+ + {}^2N^-$, $^1A'$ symmetry; (- - -) $S_8 = {}^2P^+ + {}^2N^-$, $^1A'$ symmetry.

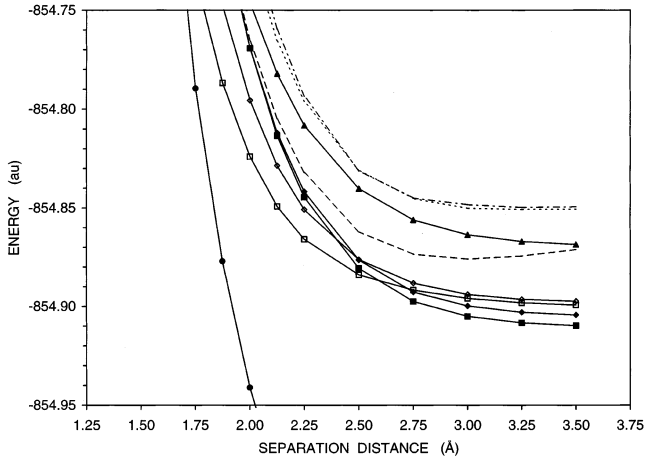


**Figure 5.** Interaction of pyrene (P) with nitromethane (N) in configuration G. States: (●) $S_0 = {}^1P_0 + {}^1N_0$, $^1A'$ symmetry; (■) $S_1 = {}^1P_1 + {}^1N_0$, $^1A'$ symmetry; (◆) $S_2 = {}^1P_2 + {}^1N_0$, $^1A''$ symmetry; (□) $S_3 = {}^1P_0 + {}^1N_1$, $^1A''$ symmetry; (◇) $S_4 = {}^1P_0 + {}^1N_2$, $^1A''$ symmetry; (− − −) $S_5 = {}^2P^+ + {}^2N^-$, $^1A'$ symmetry; (▲) $S_6 = {}^1P_3 + {}^1N_0$, $^1A''$ symmetry; (- - -) $S_7 = {}^2P^+ + {}^2N^-$, $^1A''$ symmetry; (− - −) $S_7 = {}^2P^+ + {}^2N^-$, $^1A''$ symmetry.

In the context of a fluorescence quenching experiment, the lowest-lying excited states of pyrene are populated via absorption of photons of the appropriate wavelength. The adiabatic transition energy, which is the difference between the minima of the potential energy curves for the ground and excited states of pyrene, is given in Table 2. The relatively small difference in transition energy between the first two excited states of pyrene (4.838 and 4.984 eV) as well as their disproportionate oscillator strengths (0.392 and 0.001) are consistent with what is known experimentally about the excited states of pyrene. Experimental measurements have shown that these states are accessible via one-photon excitation; the first singlet excited state (${}^1B_{2u}$) is allowed, whereas the second singlet excited state (${}^1B_{1u}$) is forbidden.[61−63] Although CIS calculations correctly predict the existence of these two states, it has been found that their order is inverted.[22] Subsequent calculations have confirmed this inversion and demonstrated that the multireference effect is crucial in predicting the correct order of the two lowest-lying singlet excited states of pyrene.[64] It has been shown experimentally, however, that excitation to the allowed singlet state

**TABLE 2: Adiabatic Transition Energies for the Pyrene−Nitromethane Complex in Configuration A[a,b]**

| initial state | symmetry | $R_i$ (Å) | $E_i$ (au) | final state | symmetry | $R_f$ (Å) | $E_f$ (au) | $\Delta E$ (eV) | symmetry allowed? | $f$ |
|---|---|---|---|---|---|---|---|---|---|---|
| $^1P_0 + {}^1N_0$ | $^1A'$ | 2.838 | −855.093 | $^1P_1 + {}^1N_0$ | $^1A'$ | 2.816 | −854.915 | 4.838 | Y | 0.392 |
| $^1P_0 + {}^1N_0$ | $^1A'$ | 2.838 | −855.093 | $^1P_2 + {}^1N_0$ | $^1A'$ | 2.828 | −854.910 | 4.984 | Y | 0.001 |
| $^1P_1 + {}^1N_0$ | $^1A'$ | 2.816 | −854.915 | $^1P_2 + {}^1N_0$ | $^1A'$ | 2.828 | −854.910 | 0.146 | Y | ? |
| $^1P_1 + {}^1N_0$ | $^1A'$ | 2.816 | −854.915 | $^1P_0 + {}^1N_1$ | $^1A''$ | 2.944 | −854.903 | 0.333 | N | ? |
| $^1P_1 + {}^1N_0$ | $^1A'$ | 2.816 | −854.915 | $^1P_0 + {}^1N_2$ | $^1A''$ | 2.865 | −854.902 | 0.365 | N | ? |
| $^1P_1 + {}^1N_0$ | $^1A'$ | 2.816 | −854.915 | $^2P^+ + {}^2N^-$ | $^1A'$ | 2.027 | −854.884 | 0.849 | Y | ? |
| $^1P_2 + {}^1N_0$ | $^1A'$ | 2.828 | −854.910 | $^2P^+ + {}^2N^-$ | $^1A'$ | 2.027 | −854.884 | 0.703 | Y | ? |
| $^1P_0 + {}^1N_1$ | $^1A''$ | 2.944 | −854.903 | $^1P_0 + {}^1N_0$ | $^1A'$ | 2.838 | −855.093 | −5.171 | N | 0.000 |
| $^1P_0 + {}^1N_2$ | $^1A''$ | 2.865 | −854.902 | $^1P_0 + {}^1N_0$ | $^1A'$ | 2.838 | −855.093 | −5.203 | N | 0.000 |
| $^2P^+ + {}^2N^-$ | $^1A'$ | 2.027 | −854.884 | $^1P_0 + {}^1N_0$ | $^1A'$ | 2.838 | −855.093 | −5.688 | Y | 0.028 |

[a] 6-31G/6-31+G. [b] $R_i$ and $R_f$ = intermolecular separation distance of optimized initial and final state; $E_i$ and $E_f$ = energy of optimized initial and final state; $\Delta E = E_f - E_i$ = adiabatic transition energy; $f$ = oscillator strength.

can result in population of the forbidden singlet state through vibrational coupling.[22,65] Therefore, it can be assumed that both of these excited states are available for deactivation by nitromethane.

As pyrene and nitromethane diffuse toward one another in solution, the energies for their various excited states change as shown in Figures 4 and 5. In some cases, the curves for these states cross, representing separation distances where an excited-state pyrene complex may undergo a transition to another electronic state. These radiationless transitions represent possible mechanisms for selective fluorescence quenching. In particular, $^1P_1 + {}^1N_0$ and $^1P_2 + {}^1N_0$ become isoenergetic with $^1P_0 + {}^1N_1$, $^1P_0 + {}^1N_2$, and $^2P^+ + {}^2N^-$. When the molecules are brought together in the attractive configuration A (Figure 4), these crossing points occur at distances of 1.625−1.875 Å. In the repulsive configuration G (Figure 5), the crossing points for the nitromethane excited states occur at farther distances of 2.35−2.75 Å, but the ion pair does not intersect until a short intermolecular distance (approximately 2.00 Å) and very high energy are reached. Note that these crossing points occur at distances less than the minima of the potential energy curves. As the energy of the ion-pair state has been shown to be sensitive to basis set (vide supra), it is likely that additional basis functions will create crossing points at larger and more energetically feasible distances. In both the attractive and repulsive configurations, the ion-pair state has a charge separation ranging from ±0.99 to ±0.85, which decreases as the separation distance decreases. The formation of a true ion pair for pyrene−nitromethane contrasts with the experimental and calculated behavior of pyrene with other quenchers such as aliphatic amines, which have been shown to form only partial charge-transfer complexes in fluorescence quenching reactions.[66,67] Finally, the intersections of the $^1P_1 + {}^1N_0$ and $^1P_2 + {}^1N_0$ surfaces with those of $^1P_0 + {}^1N_1$ and $^1P_0 + {}^1N_2$ occur at relatively the same energy in the attractive and repulsive configurations. This implies that the transition energy between excited-state pyrene and excited-state nitromethane may be relatively insensitive to molecular orientation.

To assess the likelihood of an excited-state pyrene complex undergoing a transition to either an excited-state nitromethane complex or an ion pair, both energetic and symmetry constraints can be considered. By optimizing the intermolecular separation of the attractive configuration (A), the adiabatic transition energies can be calculated between the various potential energy surfaces (Table 2). For example, the transition energy from $^1P_1 + {}^1N_0$ or $^1P_2 + {}^1N_0$ to $^1P_0 + {}^1N_1$ or $^1P_0 + {}^1N_2$ is 0.18−0.36 eV, whereas that to $^2P^+ + {}^2N^-$ is 0.70−0.85 eV. It is important to note that the transition energies to nonradiative states, particularly the ion pair, are likely to be overestimated given the limitations of the basis set and computational methods used here. With additional basis functions, the transition energies to the ion-pair state are quite likely to decrease, as discussed above.

Symmetry selection rules dictate that two electronic states must have the same symmetry in order for vibrationless ($\nu_0 - \nu_0$) transitions between those states to be allowed.[68] Accordingly, $^1P_0 + {}^1N_1$, $^1P_0 + {}^1N_2$, and $^2P^+ + {}^2N^-$ are potential partners for energy transfer with $^1P_1 + {}^1N_0$ or $^1P_2 + {}^1N_0$ in configuration A. However, only the route involving the ion pair is allowed by symmetry selection rules, despite a higher transition energy. Similarly, the only symmetry-allowed adiabatic transitions to the ground state ($^1A'$) are either fluorescence from the $^1P_1 + {}^1N_0$ or $^1P_2 + {}^1N_0$ states or recombination of the ion pair to form a neutral ground-state complex.

It is important to note that the applicability of these symmetry arguments is limited. This is true because the irreducible representation for the various excited states is dependent on the location of the $C_s$ symmetry plane for the molecular complex. Therefore, an excited state that is directly analogous in the two configurations may have a different symmetry designation depending on the location of the symmetry plane (e.g., $^1P_2 + {}^1N_0$ in Figures 4 and 5). Furthermore, rotation of the methyl group of nitromethane can alter the location of the symmetry plane and thereby change the symmetry designation. Such changes in symmetry designation, for example, cause transitions between excited-state pyrene and excited-state nitromethane to be allowed in certain molecular configurations. Last, in all cases, vibronic transitions may occur between electronic states provided that molecular vibrations of the appropriate symmetry are present. Given the complexity of this system, it is expected that a large density of vibrational states exists among the electronic states, thereby increasing the opportunities for allowed transitions. Taken together, the limitations on symmetry arguments for this system outweigh any potential insight they may offer, so further mechanistic discussions will be limited to energetic concerns.

Various similarities and differences to pyrene can be seen in the behavior of the fluoranthene−nitromethane complex. Figures 6 and 7 show the interaction of fluoranthene and nitromethane in configurations A and G, respectively. As with pyrene, the lowest-lying states represented in order of increasing energy are as follows: excited-state fluoranthene with ground-state nitromethane ($^1F_1 + {}^1N_0$, $^1F_2 + {}^1N_0$, $^1F_3 + {}^1N_0$, and $^1F_4 + {}^1N_0$), ground-state fluoranthene with excited-state nitromethane ($^1F_0 + {}^1N_1$ and $^1F_0 + {}^1N_2$), and two ion pairs consisting of a fluoranthene cation with a nitromethane anion ($^2F^+ + {}^2N^-$). Although various crossing points are seen in these potential energy surfaces, only the $^1F_2 + {}^1N_0$ and $^1F_0 + {}^1N_1$ states are involved. In addition, although an ion pair is shown to form between fluoranthene and nitromethane, it is energetically inaccessible from either the $^1F_1 + {}^1N_0$ or $^1F_2 + {}^1N_0$ surface.

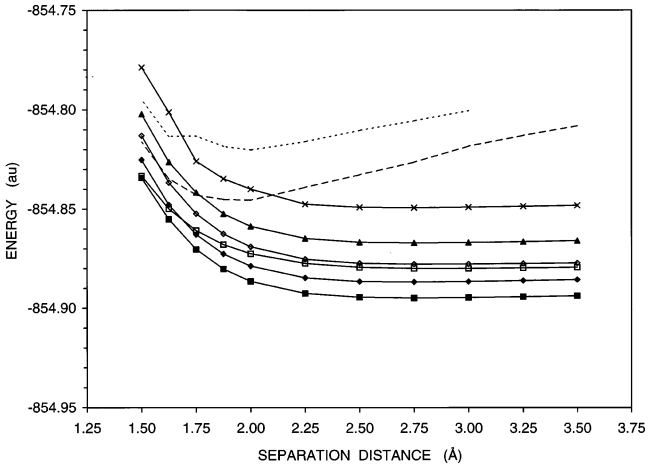


**Figure 6.** Interaction of fluoranthene (F) with nitromethane (N) in configuration A. States: (■) $S_1 = {}^1F_1 + {}^1N_0$, ${}^1A'$ symmetry; (◆) $S_2 = {}^1F_2 + {}^1N_0$, ${}^1A'$ symmetry; (□) $S_3 = {}^1F_0 + {}^1N_1$, ${}^1A''$ symmetry; (◇) $S_4 = {}^1F_0 + {}^1N_2$, ${}^1A''$ symmetry; (▲) $S_5 = {}^1F_3 + {}^1N_0$, ${}^1A'$ symmetry; (X) $S_6 = {}^1F_4 + {}^1N_0$, ${}^1A'$ symmetry; (− − −) $S_7 = {}^2F^+ + {}^2N^-$, ${}^1A'$ symmetry; (- - -) $S_8 = {}^2F^+ + {}^2N^-$, ${}^1A'$ symmetry.

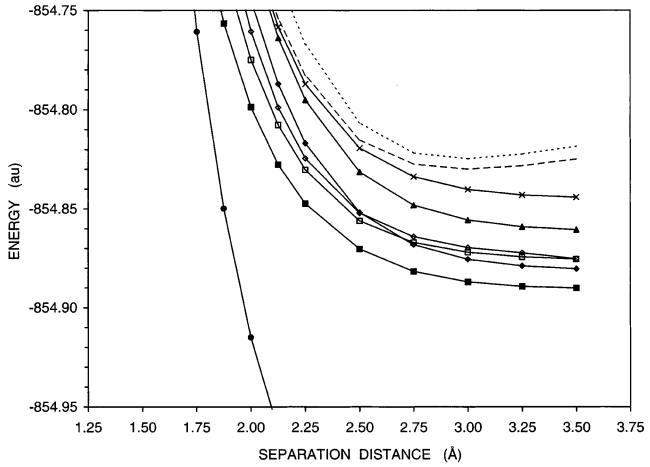


**Figure 7.** Interaction of fluoranthene (F) with nitromethane (N) in configuration G. States: (●) $S_0 = {}^1F_0 + {}^1N_0$, ${}^1A'$ symmetry; (■) $S_1 = {}^1F_1 + {}^1N_0$, ${}^1A''$ symmetry; (◆) $S_2 = {}^1F_2 + {}^1N_0$, ${}^1A'$ symmetry; (□) $S_3 = {}^1F_0 + {}^1N_1$, ${}^1A''$ symmetry; (◇) $S_4 = {}^1F_0 + {}^1N_2$, ${}^1A''$ symmetry; (▲) $S_5 = {}^1F_3 + {}^1N_0$, ${}^1A''$ symmetry; (X) $S_6 = {}^1F_4 + {}^1N_0$, ${}^1A'$ symmetry; (− − −) $S_7 = {}^2F^+ + {}^2N^-$, ${}^1A'$ symmetry; (- - -) $S_8 = {}^2F^+ + {}^2N^-$, ${}^1A''$ symmetry.

A final unique characteristic of this system is that the second ion-pair state of fluoranthene−nitromethane exhibits an avoided crossing with the ${}^1F_4 + {}^1N_0$ state. In this case, the two states exchange identities but have a discontinuity at the point of their intersection. Theories for this phenomenon have been explicitly developed for diatomic molecules, where avoided crossings are observed if the two states have identical symmetry, electronic wave functions that strongly mix, and the force of their approach (e.g., the change in the energy with separation distance) is high.[69−71] Similar discontinuities have been observed for polyatomic systems as well.[72−75] In these systems, nonadiabatic "hops" may occur between closely approaching potential energy surfaces of identical symmetry. However, these "hops" are not observed in all cases because the potential energy surfaces may have continuous or conical intersections owing to the greater degrees of freedom in the polyatomic systems. It is noteworthy that avoided crossings are often observed in computational studies of photochemical reactions.[74−77]

Adiabatic transition energies for fluoranthene−nitromethane complexes (Table 3) show similar trends to those for the pyrene−nitromethane complexes. However, major differences include higher transition energies between the ${}^1F_1 + {}^1N_0$ or ${}^1F_2 + {}^1N_0$ surfaces and other excited states, particularly the ion-pair state (1.1−1.3 eV). In addition, the transition from the ion pair thus formed to the ground state exhibits a smaller oscillator strength for fluoranthene than for pyrene (0.01 versus 0.03). Taken together, these results indicate that deactivation of fluoranthene by nitromethane can proceed via formation of an ion pair. However, this process is much less favorable than for pyrene−nitromethane.

*2. PAH−Acetonitrile Complexes.* To elucidate the origin of selective fluorescence quenching of PAHs, it is important to contrast the behavior of the quencher with that of the solvent. Solvent molecules such as methanol or acetonitrile are far more abundant than quencher molecules in solution-phase studies and ultimately limit the energy and lifetime of the excited-state fluorophore. To examine this in more detail, Figure 8 shows the interaction of pyrene and acetonitrile in the attractive configuration A. In this case, only states corresponding to excited-state pyrene with ground-state acetonitrile (${}^1P_1 + {}^1A_0$ and ${}^1P_2 + {}^1A_0$) and an ion pair consisting of a pyrene cation with an acetonitrile anion (${}^2P^+ + {}^2A^-$) are seen. Importantly, no excited-state acetonitrile states are located within a reasonable energy of the ${}^1P_1 + {}^1A_0$ and ${}^1P_2 + {}^1A_0$ surfaces, precluding direct energy transfer between pyrene and acetonitrile. As shown in Table 4, ion pairs may form between pyrene and acetonitrile. However, the transition energies from excited-state pyrene to a pyrene−acetonitrile ion pair are unfavorable (1.3−1.4 eV).

The interaction of pyrene with acetonitrile in the repulsive configuration G is shown in Figure 9. These potential energy surfaces are noticeably similar to those for the attractive configuration A, as shown in Figure 8. This demonstrates that the smaller dipole moment of acetonitrile relative to nitro-

**TABLE 3: Adiabatic Transition Energies for the Fluoranthene−Nitromethane Complex in Configuration A[a,b]**

| initial state | symmetry | $R_i$ (Å) | $E_i$ (au) | final state | symmetry | $R_f$ (Å) | $E_f$ (au) | $\Delta E$ (eV) | symmetry allowed? | $f$ |
|---|---|---|---|---|---|---|---|---|---|---|
| ${}^1F_0 + {}^1N_0$ | ${}^1A'$ | 2.759 | −855.070 | ${}^1F_1 + {}^1N_0$ | ${}^1A'$ | 2.737 | −854.895 | 4.759 | Y | 0.012 |
| ${}^1F_0 + {}^1N_0$ | ${}^1A'$ | 2.759 | −855.070 | ${}^1F_2 + {}^1N_0$ | ${}^1A'$ | 2.709 | −854.887 | 4.978 | Y | 0.425 |
| ${}^1F_1 + {}^1N_0$ | ${}^1A'$ | 2.737 | −854.895 | ${}^1F_2 + {}^1N_0$ | ${}^1A'$ | 2.709 | −854.887 | 0.219 | Y | ? |
| ${}^1F_1 + {}^1N_0$ | ${}^1A'$ | 2.737 | −854.895 | ${}^1F_0 + {}^1N_1$ | ${}^1A''$ | 2.861 | −854.880 | 0.404 | N | ? |
| ${}^1F_1 + {}^1N_0$ | ${}^1A'$ | 2.737 | −854.895 | ${}^1F_0 + {}^1N_2$ | ${}^1A''$ | 2.825 | −854.878 | 0.464 | N | ? |
| ${}^1F_1 + {}^1N_0$ | ${}^1A'$ | 2.737 | −854.895 | ${}^2F^+ + {}^2N^-$ | ${}^1A'$ | 1.966 | −854.845 | 1.344 | Y | ? |
| ${}^1F_2 + {}^1N_0$ | ${}^1A'$ | 2.709 | −854.887 | ${}^2F^+ + {}^2N^-$ | ${}^1A'$ | 1.966 | −854.845 | 1.126 | Y | ? |
| ${}^1F_0 + {}^1N_1$ | ${}^1A''$ | 2.861 | −854.880 | ${}^1F_0 + {}^1N_0$ | ${}^1A'$ | 2.759 | −855.070 | −5.163 | N | 0.000 |
| ${}^1F_0 + {}^1N_2$ | ${}^1A''$ | 2.825 | −854.878 | ${}^1F_0 + {}^1N_0$ | ${}^1A'$ | 2.759 | −855.070 | −5.223 | N | 0.000 |
| ${}^2F^+ + {}^2N^-$ | ${}^1A'$ | 1.966 | −854.845 | ${}^1F_0 + {}^1N_0$ | ${}^1A'$ | 2.759 | −855.070 | −6.103 | Y | 0.011 |

[a] 6-31G/6-31+G. [b] $R_1$ and $R_f$ = intermolecular separation distance of optimized initial and final state; $E_i$ and $E_f$ = energy of optimized initial and final state; $\Delta E = E_f - E_i$ = adiabatic transition energy; $f$ = oscillator strength.

**TABLE 4: Adiabatic Transition Energies for the Pyrene−Acetonitrile Complex in Configuration A[a,b]**

| initial state | symmetry | $R_i$ (Å) | $E_i$ (au) | final state | symmetry | $R_f$ (Å) | $E_f$ (au) | $\Delta E$ (eV) | symmetry allowed? | $f$ |
|---|---|---|---|---|---|---|---|---|---|---|
| $^1P_0 + {}^1A_0$ | $^1A'$ | 3.039 | −743.427 | $^1P_1 + {}^1A_0$ | $^1A'$ | 3.017 | −743.249 | 4.839 | Y | 0.408 |
| $^1P_0 + {}^1A_0$ | $^1A'$ | 3.039 | −743.427 | $^1P_2 + {}^1A_0$ | $^1A'$ | 3.025 | −743.244 | 4.983 | Y | 0.001 |
| $^1P_1 + {}^1A_0$ | $^1A'$ | 3.017 | −743.249 | $^1P_2 + {}^1A_0$ | $^1A'$ | 3.025 | −743.244 | 0.144 | Y | ? |
| $^1P_1 + {}^1A_0$ | $^1A'$ | 3.017 | −743.249 | $^2P^+ + {}^2A^-$ | $^1A''$ | 2.411 | −743.195 | 1.456 | N | ? |
| $^1P_2 + {}^1A_0$ | $^1A'$ | 3.025 | −743.244 | $^2P^+ + {}^2A^-$ | $^1A''$ | 2.411 | −743.195 | 1.312 | N | ? |
| $^2P^+ + {}^2A^-$ | $^1A''$ | 2.411 | −743.195 | $^1P_0 + {}^1A_0$ | $^1A'$ | 3.039 | −743.427 | −6.295 | N | 0.003 |

[a] 6-31G/6-31+G. [b] $R_1$ and $R_f$ = intermolecular separation distance of optimized initial and final state; $E_i$ and $E_f$ = energy of optimized initial and final state; $\Delta E = E_f - E_i$ = adiabatic transition energy; $f$ = oscillator strength.

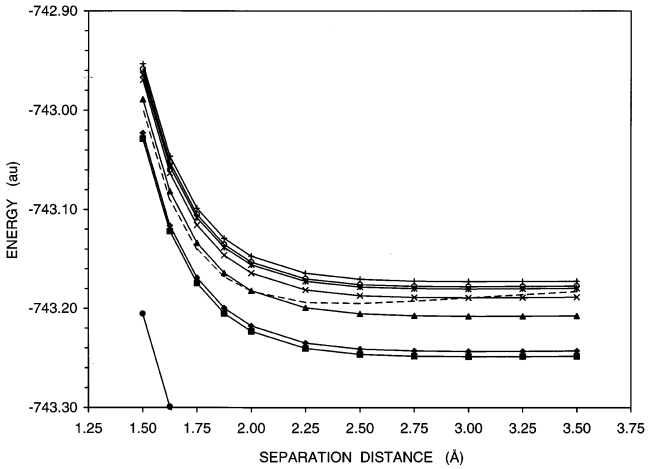


**Figure 8.** Interaction of pyrene (P) with acetonitrile (A) in configuration A. States: (●) $S_0 = {}^1P_0 + {}^1A_0$, $^1A'$ symmetry; (■) $S_1 = {}^1P_1 + {}^1A_0$, $^1A'$ symmetry; (◆) $S_2 = {}^1P_2 + {}^1A_0$, $^1A'$ symmetry; (▲) $S_3 = {}^1P_3 + {}^1A_0$, $^1A'$ symmetry; (X) $S_4 = {}^1P_4 + {}^1A_0$, $^1A'$ symmetry; (− − −) $S_5 = {}^2P^+ + {}^2A^-$, $^1A''$ symmetry; (*) $S_6 = {}^1P_5 + {}^1A_0$, $^1A'$ symmetry; (○) $S_7 = {}^1P_6 + {}^1A_0$, $^1A'$ symmetry; (+) $S_8 = {}^1P_7 + {}^1A_0$, $^1A'$ symmetry.

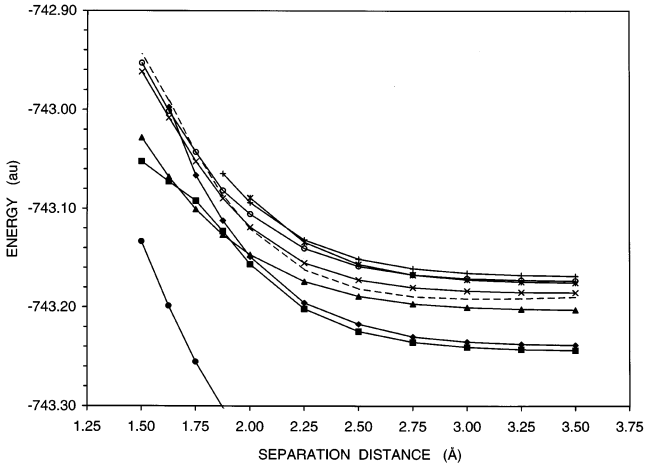


**Figure 9.** Interaction of pyrene (P) with acetonitrile (A) in configuration G. States: (●) $S_0 = {}^1P_0 + {}^1A_0$, $^1A'$ symmetry; (■) $S_1 = {}^1P_1 + {}^1A_0$, $^1A'$ symmetry; (◆) $S_2 = {}^1P_2 + {}^1A_0$, $^1A''$ symmetry; (▲) $S_3 = {}^1P_3 + {}^1A_0$, $^1A''$ symmetry; (− − −) $S_4 = {}^2P^+ + {}^2A^-$, $^1A''$ symmetry; (X) $S_5 = {}^1P_4 + {}^1A_0$, $^1A''$ symmetry; (*) $S_6 = {}^1P_5 + {}^1A_0$, $^1A''$ symmetry; (○) $S_7 = {}^1P_6 + {}^1A_0$, $^1A'$ symmetry; (+) $S_8 = {}^1P_7 + {}^1A_0$, $^1A'$ symmetry.

methane reduces the influence of molecular orientation on the energy of the complex. Of further note is an avoided crossing between the $^1P_2 + {}^1A_0$ and $^1P_3 + {}^1A_0$ surfaces. As this is a transition between excited states of pyrene, it represents a perturbation of the fluorescence emission by internal conversion rather than by deactivation or quenching of the pyrene molecule.

Finally, Figures 10 and 11 show the interaction of fluoranthene and acetonitrile in configurations A and G, respectively.

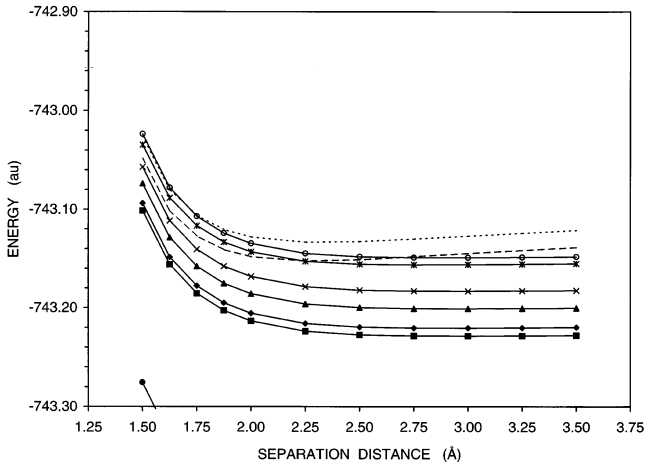


**Figure 10.** Interaction of fluoranthene (F) with acetonitrile (A) in configuration A. States: (●) $S_0 = {}^1F_0 + {}^1A_0$, $^1A'$ symmetry; (■) $S_1 = {}^1F_1 + {}^1A_0$, $^1A'$ symmetry; (◆) $S_2 = {}^1F_2 + {}^1A_0$, $^1A'$ symmetry; (▲) $S_3 = {}^1F_3 + {}^1A_0$, $^1A'$ symmetry; (X) $S_4 = {}^1F_4 + {}^1A_0$, $^1A'$ symmetry; (*) $S_5 = {}^1F_5 + {}^1A_0$, $^1A'$ symmetry; (○) $S_6 = {}^1F_6 + {}^1A_0$, $^1A'$ symmetry; (− − −) $S_7 = {}^2F^+ + {}^2A^-$, $^1A''$ symmetry; (- - -) $S_8 = {}^2F^+ + {}^2A^-$, $^1A'$ symmetry.

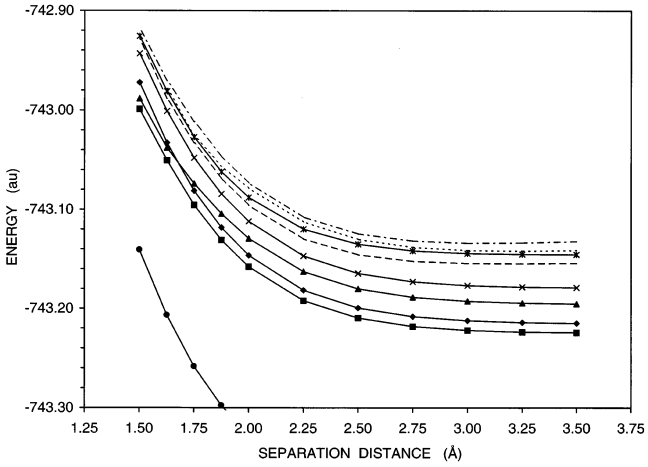


**Figure 11.** Interaction of fluoranthene (F) with acetonitrile (A) in configuration G. States: (●) $S_0 = {}^1F_0 + {}^1A_0$, $^1A'$ symmetry; (■) $S_1 = {}^1F_1 + {}^1A_0$, $^1A''$ symmetry; (◆) $S_2 = {}^1F_2 + {}^1A_0$, $^1A'$ symmetry; (▲) $S_3 = {}^1F_3 + {}^1A_0$, $^1A''$ symmetry; (X) $S_4 = {}^1F_4 + {}^1A_0$, $^1A'$ symmetry; (− − −) $S_5 = {}^2F^+ + {}^2A^-$, $^1A''$ symmetry; (*) $S_6 = {}^1F_5 + {}^1A_0$, $^1A'$ symmetry; (- - -) $S_7 = {}^1F_6 + {}^1A_0$, $^1A''$ symmetry; (− - −) $S_8 = {}^2F^+ + {}^2A^-$, $^1A'$ symmetry.

The calculated potential energy surfaces for fluoranthene−acetonitrile demonstrate the same trends as those for pyrene−acetonitrile. There are very few crossing points and no opportunities for energy transfer to either excited-state acetonitrile or fluoranthene−acetonitrile ion pairs. Also, as shown in Table 5, there is a larger barrier for formation of a fluoranthene−acetonitrile ion pair (1.8−2.1 eV).

**TABLE 5: Adiabatic Transition Energies for the Fluoranthene−Acetonitrile Complex in Configuration A[a,b]**

| initial state | symmetry | $R_i$ (Å) | $E_i$ (au) | final state | symmetry | $R_f$ (Å) | $E_f$ (au) | $\Delta E$ (eV) | symmetry allowed? | $f$ |
|---|---|---|---|---|---|---|---|---|---|---|
| $^1F_0 + {}^1A_0$ | $^1A'$ | 2.930 | −743.404 | $^1F_1 + {}^1A_0$ | $^1A'$ | 2.914 | −743.229 | 4.760 | Y | 0.013 |
| $^1F_0 + {}^1A_0$ | $^1A'$ | 2.930 | −743.404 | $^1F_2 + {}^1A_0$ | $^1A'$ | 2.886 | −743.221 | 4.979 | Y | 0.442 |
| $^1F_1 + {}^1A_0$ | $^1A'$ | 2.914 | −743.229 | $^1F_2 + {}^1A_0$ | $^1A'$ | 2.886 | −743.221 | 0.219 | Y | ? |
| $^1F_1 + {}^1A_0$ | $^1A'$ | 2.914 | −743.229 | $^2F^+ + {}^2A^-$ | $^1A''$ | 2.275 | −743.153 | 2.074 | N | ? |
| $^1F_2 + {}^1A_0$ | $^1A'$ | 2.886 | −743.221 | $^2F^+ + {}^2A^-$ | $^1A''$ | 2.275 | −743.153 | 1.855 | N | ? |
| $^2F^+ + {}^2A^-$ | $^1A''$ | 2.275 | −743.153 | $^1F_0 + {}^1A_0$ | $^1A'$ | 2.930 | −743.404 | −6.834 | N | 0.000 |

[a] 6-31G/6-31+G. [b] $R_1$ and $R_f$ = intermolecular separation distance of optimized initial and final state; $E_i$ and $E_f$ = energy of optimized initial and final state; $\Delta E = E_f - E_i$ = adiabatic transition energy; $f$ = oscillator strength.

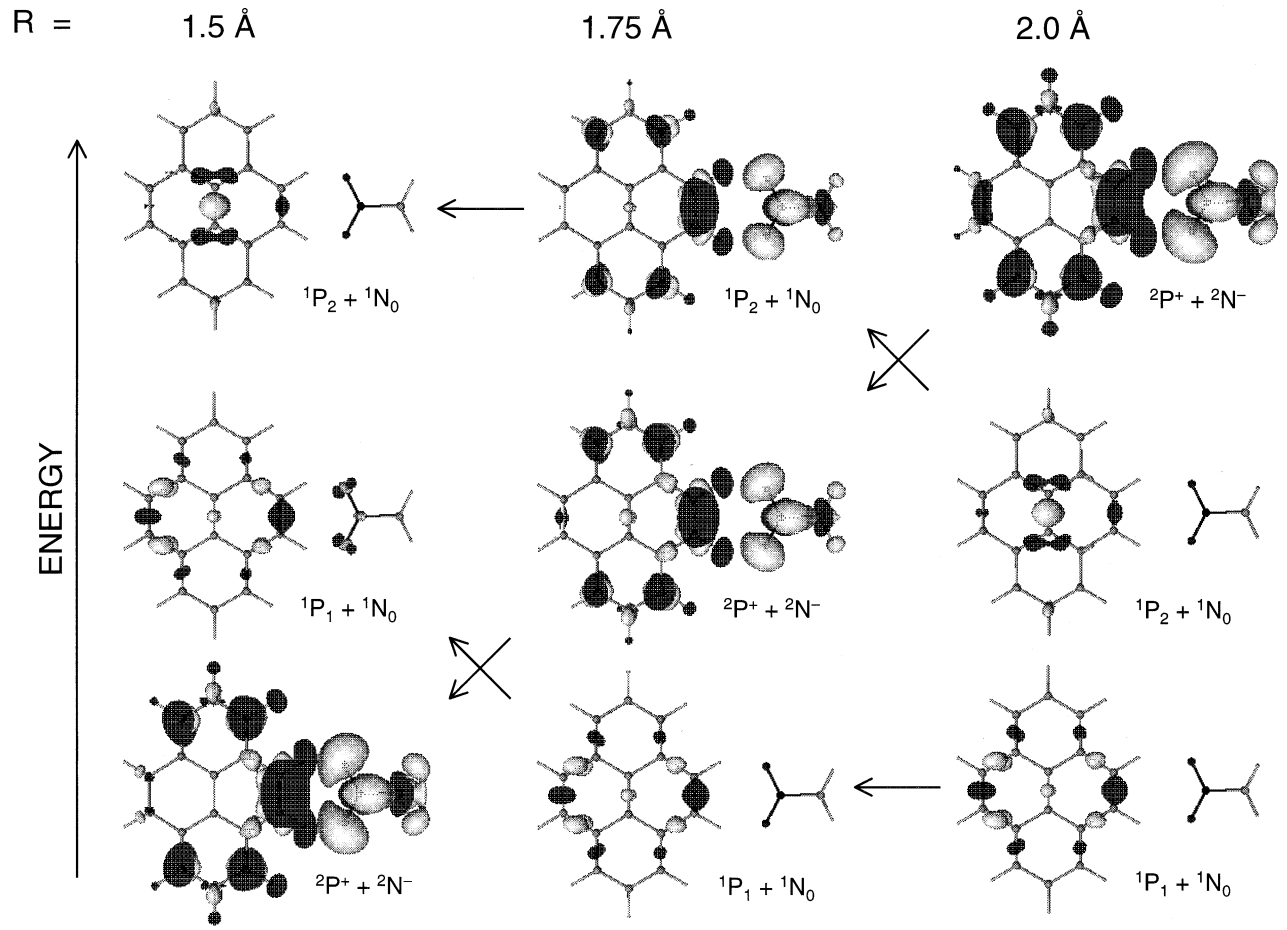


**Figure 12.** Visualization of the electron density changes for two excited-state singlets of pyrene ($^1P_1 + {}^1N_0$ and $^1P_2 + {}^1N_0$) and a pyrene−nitromethane ion pair ($^2P^+ + {}^2N^-$) in configuration A as a function of intermolecular separation distance.

**D. Triplet-State Potential Energy Surfaces.** The mechanisms for selective fluorescence quenching discussed above only consider interactions between singlet states of the fluorophore and quencher. However, it is also possible to deactivate a singlet-state fluorophore by internal conversion to a triplet state. This process is especially prevalent in fluorophores or quenchers that contain atoms with a high atomic number (the heavy atom effect), where electron spin and orbital motions are efficiently coupled.[78,79] The consequence of this spin−orbit coupling is mixing of electronic states with different multiplicity, which facilitates intersystem crossing from the singlet to triplet state. In fact, one of the earliest applications of fluorescence quenching was the use of iodomethane and iodoethane to enhance intersystem crossing and thereby increase the phosphorescence yield of selected PAHs.[1,80]

To investigate their possible role, the triplet-state potential energy surfaces have been calculated for pyrene−nitromethane and fluoranthene−nitromethane in configuration A. Various excited-state triplets are comparable in energy to the low-lying singlets of pyrene−nitromethane, including triplet states of pyrene ($^3P_x + {}^1N_0$) and triplet states of nitromethane ($^1P_0 + {}^3N_x$). In addition, at small separation distances (1.5 Å), a triplet ion pair ($^2P^+ + {}^2N^-$) appears in which the unpaired electrons have the same, rather than opposite, spin. Energetically, these triplet states are accessible from the singlet states of pyrene that are expected to be populated by absorption of photons ($^1P_1 + {}^1N_0$ or $^1P_2 + {}^1N_0$). Intersystem crossing to either the neutral or ionic triplet states could lead to the quenching of fluorescence by promotion of phosphorescence or by deactivation of the longer-lived triplet states through subsequent collisions with ground-state quencher molecules.

Excited-state triplets of fluoranthene−nitromethane are also comparable in energy to the low-lying singlets of this complex, including triplet states of fluoranthene ($^3F_x + {}^1N_0$) and triplet states of nitromethane ($^1F_0 + {}^3N_x$). However, unlike pyrene−nitromethane, no triplet ion pair is observed. These results

suggest that, as with the singlet excited states, selective deactivation of excited-state PAHs via a triplet-state intermediate involves electron transfer. However, transitions between singlet and triplet states are forbidden by spin selection rules for both pyrene and fluoranthene and neither the fluorophore nor quencher has heavy atoms to promote intersystem crossing. Therefore, the overall likelihood of this deactivation mechanism is low.

**E. Visualization of Ion-Pair Formation.** As a final illustration of the quenching phenomenon and its potential quantum chemical mechanism, the electron density differences between the ground and excited states of pyrene−nitromethane are visualized in configuration A. As shown in Figure 12, three singlet excited states are portrayed at various separation distances with their relative energies reflected in their placement on the vertical axis. Areas where the electron density increases from the ground state are shaded in white, whereas areas where the electron density decreases are shaded in black. At large separation distances, the two lowest-lying excited states can be identified as singlet states of pyrene ($^1P_1 + {}^1N_0$ or $^1P_2 + {}^1N_0$, respectively). Changes in electron density are localized on the pyrene molecule and reflect its excitation character.[22] In contrast, the third excited state can be identified as a pyrene−nitromethane ion pair ($^2P^+ + {}^2N^-$). There is a large decrease in charge on the pyrene molecule and a similarly large increase in charge on the nitromethane molecule.

As the intermolecular separation distance is reduced, the relative energies of these states change. For example, when the molecules are at a separation distance of 1.75 Å, the energy of $^1P_2 + {}^1N_0$ and the ion pair converge. Concomitantly, there is strong mixing of the excitation character of these two states. This implies that in the quenching mechanism, ionization of this particular singlet state of pyrene may initiate the deactivation process. As the molecules approach one another, the ion pair continues to decrease in energy with respect to the other excited states, eventually becoming the lowest lying singlet at a separation distance of 1.5 Å.

## IV. Summary

The use of ab initio techniques to elucidate the photophysical mechanism of selective fluorescence quenching is a powerful and novel approach for studying a long observed but poorly understood phenomenon. The importance of accurately simulating the diffuse electron density of the neutral and anionic states of the quencher has been demonstrated. Specifically, the relative energy of the ionic states is much reduced upon the addition of diffuse functions to the atoms of the quencher molecule. As electron transfer appears to be the basis for the selective deactivation of alternant fluorophores such as pyrene, inclusion of diffuse basis functions on the atoms of the fluorophore as well as the quencher would serve to account more accurately for these interactions.

Using standard configurations of pyrene, fluoranthene, nitromethane, and acetonitrile, the nature of their molecular complexes has been detailed. In particular, the magnitude and orientation of the dipole moment of either nitromethane or acetonitrile with respect to the electron density of the PAH is critical in determining the energy of attraction or repulsion. In the case of nitromethane, the formation of planar complexes such as A, B, and C in Figure 1 appears to be highly favored and may indicate the preferred orientation of quencher molecules within the solvent cage of the excited-state fluorophore.

Studies of the interaction of the PAHs with nitromethane as a function of distance show that fluorescence quenching has two possible mechanisms: direct energy transfer from the excited-state fluorophore to produce excited-state quencher or formation of an excited-state fluorophore−quencher ion pair. Both mechanisms are energetically feasible for the alternant isomer pyrene, but only direct energy transfer is possible for the nonalternant isomer fluoranthene. Furthermore, symmetry selection rules for vibrationless electronic transitions dictate that formation of the ion pair is allowed, whereas direct energy transfer is forbidden. These results suggest that, other than fluorescence, the most viable route to the ground state for an excited-state pyrene molecule is through the formation of an ion pair with nitromethane. Similar studies with acetonitrile clearly show that ion-pair formation is not energetically favorable. This is in agreement with experimental results, which show that nitromethane selectively deactivates alternant PAHs such as pyrene, whereas acetonitrile demonstrates no such ability.[1,16−18] However, the calculations described here use a modest basis set without BSSE correction, do not include electron correlation or molecular vibrations, and are analogous to the gas phase. Given these limitations, quantitative prediction of solution-phase behavior has not been attempted. It is expected that the inclusion of a model for solvation of the excited-state complexes would enable more accurate prediction of solution-phase quenching constants and the identification of promising novel quenchers.

**Acknowledgment.** The authors acknowledge Dr. Robert Bohn of the Mathematical and Computational Sciences Division at the National Institute of Standards and Technology for assistance with BSSE calculations and visualizations. Computing resources were provided by the National Science Foundation under instrument Grant CHE-9974834, and computing time was provided by the National Partnership for Advanced Computational Infrastructure. This material is based upon work supported by a National Science Foundation Graduate Fellowship and an A.C.S. Division of Analytical Chemistry Graduate Fellowship sponsored by Eli Lilly to J.V.G.

## References and Notes

(1) Lee, M. L.; Novotny; M. V.; Bartle, K. D. *Analytical Chemistry of Polycyclic Aromatic Compounds*; Academic Press: New York, 1981.
(2) Leger, A.; Puget, J. L. *Astron. Astrophys.* **1984**, *137*, L5.
(3) Allamandola, L. J.; Tielens, A. G.; Baker, J. R. *Astrophys. J.* **1985**, *290*, L25.
(4) Kershaw, J. R.; Fetzer, J. C. *Polycyclic Aromat. Compd.* **1997**, *7*, 253.
(5) Vo-Dinh, T.; Suter, G. W.; Kallir, A. J.; Wild, U. P. *J. Phys. Chem.* **1985**, *89*, 3026.
(6) Ariese, F.; Gooijer, C.; Velthorst, N. H. In *Environmental Analysis: Techniques, Applications and Quality Assurance*; Barcelo, D., Ed.; Elsevier: Amsterdam, 1993; Chapter 13.
(7) Inman, E. L., Jr.; Jurgensen, A.; Winefordner, J. D. *Analyst* **1982**, *107*, 538.
(8) Kozin, I. S.; Gooijer, C.; Velthorst, N. H. *Anal. Chim. Acta* **1996**, *333*, 193.
(9) Douglas, G. S.; Lieberman, S. H.; McGinnis, W. C.; Knowles, D.; Peven, C. *Proceedings of the International Symposium on Field Screening Methods for Hazardous Wastes and Toxic Chemicals*; Air & Waste Management Association: Pittsburgh, PA, 1995; p 837.
(10) Roch, Th.; Loehmannsroebe, H. G.; Meyer, Th. *Proc. SPIE-Int. Soc. Opt. Eng.* **1995**, *2504*, 453.
(11) Stevenson, C. L.; Vo-Dinh, T. *Anal. Chim. Acta* **1995**, *303*, 247.
(12) Fogarty, M. P.; Warner, I. M. *Appl. Spectrosc.* **1982**, *36*, 460.
(13) McGown, L. B.; Hemmingson, S. L.; Shaver, J. M.; Geng, L. *Appl. Spectrosc.* **1995**, *49*, 60.
(14) Shaver, J. M.; McGown, L. B. *Appl. Spectrosc.* **1995**, *49*, 813.
(15) Sawicki, E.; Stanley, T. W.; Elbert, W. C. *Talanta* **1964**, *11*, 1433.
(16) Chen, S. H.; Evans, C. E.; McGuffin, V. L. *Anal. Chim. Acta* **1991**, *246*, 65.
(17) Ogasawara, F. K.; Wang, Y.; McGuffin, V. L. *Appl. Spectrosc.* **1995**, *49*, 1.

(18) Goodpaster, J. V.; McGuffin, V. L. *Appl. Spectrosc.* **1999**, *53*, 1000.
(19) Rehm, D.; Weller, A. *Isr. J. Chem.* **1970**, *8*, 259.
(20) Yates, K. *Hückel Molecular Orbital Theory*; Academic Press: New York, 1978.
(21) Breymann, U.; Dreeskamp, H.; Koch, E.; Zander, M. *Chem. Phys. Lett.* **1978**, *59*, 68.
(22) Goodpaster, J. V.; Harrison, J. F.; McGuffin, V. L. *J. Phys. Chem. A* **1998**, *102*, 3372.
(23) Chung, A. H.; Dewar, D. S. *J. Chem. Phys.* **1965**, *42*, 756.
(24) Hites, R. A.; Simonsick, W. J. *Calculated Molecular Properties of Polycyclic Aromatic Hydrocarbons*; Elsevier: Amsterdam, 1987.
(25) Plummer, B. F.; Steffen, L. K.; Herndon, W. C. *Struct. Chem.* **1993**, *4*, 279.
(26) Rabinowitz, J. R.; Little, S. B. *Int. J. Quantum Chem.* **1994**, *52*, 681.
(27) Kao, J.; Allinger, N. L. *J. Am. Chem. Soc.* **1977**, *99*, 975.
(28) Kao, J. *J. Am. Chem. Soc.* **1987**, *109*, 3817.
(29) Schulman, J. M.; Peck, R. C.; Disch, R. L. *J. Am. Chem. Soc.* **1989**, *111*, 5675.
(30) Peck, R. C.; Schulman, J. M.; Disch, R. L. *J. Phys. Chem.* **1990**, *94*, 6637.
(31) Pauzat, F.; Talbi, D.; Miller, M. D.; DeFrees, D. J.; Ellinger, Y. *J. Phys. Chem.* **1992**, *96*, 7882.
(32) Vala, M.; Szczepanski, J.; Pauzat, F.; Parisel, O.; Talbi, D.; Ellinger, Y. *J. Phys. Chem.* **1994**, *98*, 9187.
(33) Langhoff, S. R. *J. Phys. Chem.* **1996**, *100*, 2819.
(34) Zakrzewski, V. G.; Dolgounitcheva, O.; Ortiz, J. V. *J. Chem. Phys.* **1996**, *105*, 8748.
(35) Nishimoto, K.; Forster, L. S. *Theor. Chim. Acta* **1965**, *3*, 407.
(36) Nishimoto, K. *Theor. Chim. Acta* **1967**, *7*, 207.
(37) Pucci, R.; Baldo, M.; Martin-Rodero, A.; Piccitto, G.; Tomasello, P. *Int. J. Quantum Chem.* **1984**, *26*, 783.
(38) Das Gupta, N. K.; Birss, F. W. *Bull. Chem. Soc. Jpn.* **1978**, *51*, 1211.
(39) Das Gupta, A.; Chatterjee, S.; Das Gupta, N. K. *Bull. Chem. Soc. Jpn.* **1979**, *52*, 3070.
(40) Sühnel, J.; Kempka, U.; Gustav, K. *J. Prakt. Chem.* **1980**, *322*, 649.
(41) Mekenyan, O. G.; Ankley, G. T.; Veith, G. D.; Call, D. J. *SAR QSAR Environ. Res.* **1994**, *2*, 237.
(42) Du, P.; Salama, F.; Loew, G. H. *Chem. Phys.* **1993**, *173*, 421.
(43) Negri, F.; Zgierski, Z. *J. Chem. Phys.* **1994**, *100*, 1387.
(44) Niederalt, C.; Grimme, S.; Peyerimhoff, S. D. *Chem. Phys. Lett.* **1995**, *245*, 455.
(45) Negri, F.; Zgierski, M. Z. *J. Chem. Phys.* **1996**, *104*, 3486.
(46) Hirata, S.; Lee, T. J.; Head-Gordon, M. *J. Chem. Phys.* **1999**, *111*, 8904.
(47) Chen, S. H.; McGuffin, V. L. *Appl. Spectrosc.* **1994**, *48*, 596.
(48) Gittins, C. M.; Rohlfing, E. A.; Rohlfing, C. M. *J. Chem. Phys.* **1996**, *105*, 7323.
(49) Berlman, I. B. *J. Phys. Chem.* **1970**, *74*, 3085.
(50) Reiling, S.; Basnard, M.; Bopp, P. A. *J. Phys. Chem. A* **1997**, *101*, 4409.
(51) Martin, N. H.; Allen, N. W., III; Cottle, C. A.; Marschke, C. K., Jr. *J. Photochem. Photobiol. A.: Chem.* **1997**, *103*, 33.
(52) Cave, R. J.; Newton, M. D. *J. Chem. Phys.* **1997**, *106*, 9213.
(53) Su, J. T.; Zewail, A. H. *J. Phys. Chem. A* **1998**, *102*, 4082.
(54) Heard, G. L.; Boyd, R. J. *J. Phys. Chem. A* **1997**, *101*, 5374.
(55) Ohta, T.; Kuroda, H.; Kunii, T. L. *Theor. Chim. Acta* **1970**, *19*, 167.
(56) Tramer, A.; Brenner, V.; Millie, P.; Piuzzi, F. *J. Phys. Chem. A* **1998**, *102*, 2798.
(57) Frisch, M. J.; Trucks, G. W.; Schlegel, H. B.; Scuseria, G. E.; Robb, M. A.; Cheeseman, J. R.; Zakrzewski, V. G.; Montgomery, J. A., Jr.; Stratmann, R. E.; Burant, J. C.; Dapprich, S.; Millam, J. M.; Daniels, A. D.; Kudin, K. N.; Strain, M. C.; Farkas, O.; Tomasi, J.; Barone, V.; Cossi, M.; Cammi, R.; Mennucci, B.; Pomelli, C.; Adamo, C.; Clifford, S.; Ochterski, J.; Petersson, G. A.; Ayala, P. Y.; Cui, Q.; Morokuma, K.; Malick, D. K.; Rabuck, A. D.; Raghavachari, K.; Foresman, J. B.; Cioslowski, J.; Ortiz, J. V.; Stefanov, B. B.; Liu, G.; Liashenko, A.; Piskorz, P.; Komaromi, I.; Gomperts, R.; Martin, R. L.; Fox, D. J.; Keith, T.; Al-Laham, M. A.; Peng, C. Y.; Nanayakkara, A.; Gonzalez, C.; Challacombe, M.; Gill, P. M. W.; Johnson, B. G.; Chen, W.; Wong, M. W.; Andres, J. L.; Head-Gordon, M.; Replogle, E. S.; Pople, J. A. *Gaussian 98*, revision A.7; Gaussian, Inc.: Pittsburgh, PA, 1998.
(58) Jansen, H. B.; Ross, P. *Chem. Phys. Lett.* **1969**, *3*, 140.
(59) Boys, S. B.; Bernardi, F. *J. Mol. Phys.* **1970**, *19*, 553.
(60) Salvador, P.; Paizs, B.; Duran, M.; Suhai, S. *J. Comput. Chem.* **2001**, *22*, 765.
(61) Ohta, N.; Baba, H.; Marconi, G. *Chem. Phys. Lett.* **1987**, *133*, 222.
(62) Marconi, G.; Salvi, P. R. *Chem. Phys. Lett.* **1986**, *123*, 254.
(63) Becker, R. S.; Singh, I. S.; Jackson, E. A. *J. Chem. Phys.* **1963**, *38*, 2144.
(64) Bito, Y.; Shida, N.; Toru, T. *Chem. Phys. Lett.* **2000**, *328*, 310.
(65) Borisevich, N. A.; Vodovatov, L. B.; D'yachenko, G. G.; Petukhov, V. A.; Semyonov, M. A. *J. Appl. Spectrosc.* **1995**, *62*, 482.
(66) Andrews, D. P.; Beddard, G. S.; Whitaker, B. J. *J. Phys. Chem. A* **2000**, *104*, 7785.
(67) Sinicropi, A.; Pischel, U.; Basosi, R.; Nau, W. M.; Olivucci, M. *Angew. Chem. Int. Ed.* **2000**, *39*, 4582.
(68) Gilbert, A.; Baggott, J. *Essentials of Molecular Photochemistry*; CRC Press: Boca Raton, FL, 1991; p 128.
(69) Landau, L. D.; Lifshitz, E. M. *Quantum Mechanics: Non-Relativistic Theory*, 2nd ed.; Sykes, J. B., Bell, J. S., Eds.; Trans., Pergamon Press: New York, 1965; pp 322−331.
(70) Nikitin, E. E.; Umanskii, S. Ya. *Theory of Slow Atomic Collisions*; Springer-Verlag: New York, 1979; pp 273−312.
(71) Steinfeld, J. I.; Francisco, J. S.; Hase, W. L. *Chemical Kinetics and Dynamics*; Prentice Hall: Englewood Cliffs, NJ, 1989; pp 237−245.
(72) Ohrendorf, E.; Cederbaum, L. S.; Koppel, H. *Chem. Phys. Lett.* **1988**, *151*, 273.
(73) Allison, T. C.; Mielke, S. L.; Schwenke, D. W.; Truhlar, D. G. *J. Chem. Soc., Faraday Trans.* **1997**, *93*, 825.
(74) Boggio-Pasqua, M.; Bearpark, M. J.; Hunt, P. A.; Robb, M. A. *J. Am. Chem. Soc.* **2002**, *124*, 1456.
(75) Sinicropi, A.; Pogni, R.; Basosi, R.; Robb, M. A.; Gramlich, G.; Nau, W. M.; Olivucci, M. *Angew. Chem., Int. Ed.* **2001**, *40*, 4185.
(76) Devaquet, A.; Sevin, A.; Bigot, B. *J. Am. Chem. Soc.* **1978**, *100*, 2009.
(77) Bernardi, F.; Olivucci, M.; Robb, M. *Isr. J. Chem.* **1993**, *33*, 265.
(78) Badley, R. *Fluorescence Spectroscopy*; Plenum Press: New York, 1983.
(79) Lakowicz, J. *Principles of Fluorescence Spectroscopy*; Plenum Press: New York, 1983.
(80) Vo-Dinh, T. *Chemical Analysis of Polycyclic Aromatic Compounds*; John Wiley and Sons: New York, 1989.